PFC/JA-88-20

Stability of Plasmas Sustained by ICRF in the Central Cell of the Tara Tandem Mirror

S. N. Golovato, K. Brau, J. Casey, M. J. Gerver,
S. Horne, J. Irby, J. Kesner, B. Lane, J. Machuzak,
R. Myer, R. S. Post, E. Sevillano, L. Wang

Plasma Fusion Center
Massachusetts Institute of Technology
Cambridge, MA 02139

May 1988

Submitted to: Physics of Fluids

This work was supported by the U. S. Department of Energy Contract No. DE-AC02-78ET51013. Reproduction, translation, publication, use and disposal, in whole or in part by or for the United States government is permitted.

ABSTRACT

The stability of plasmas produced by ICRF slow wave excitation using a slot antenna has been studied in the central cell of the Tara tandem mirror. ICRF provided stability against macroscopic plasma motions in an axisymmetric configuration. The maintenance of macroscopic stability depended on the gas fueling rate, ion cyclotron resonance location, and ω/ω_{ci} at the antenna location. The ICRF ponderomotive force model is consistent with many of the observed stability features and predicts that the E_+ component of the ICRF was responsible for the stabilization. The Alfvén ion cyclotron micro-instability was observed when the plasma $\beta_\perp$ and anisotropy were sufficiently high. Probe measurements of the unstable mode identified it as an ion cyclotron wave and the instability threshold was within a factor of two of the predicted value.

I. INTRODUCTION

Stability has often limited plasma confinement in mirror systems to levels substantially below the limitation imposed by end loss. Magnetohydrodynamic (MHD) theory predicts that stability to low frequency (frequency, $\omega \ll$the ion cyclotron frequency, ω_{ci}), macroscopic plasma displacements can be provided by absolute minimum-$|B|$ geometry [1] or pressure-weighted $\int dl/B$.[2] These techniques usually require regions of non-axisymmetric magnetic field, which have been shown to lead to enhanced radial transport.[3,4] The use of internal coils to provide stable (good) field line curvature in axisymmetric geometry can provide stability at the expense of particle losses to the coils and coil supports.[5,6] Plasmas produced by radio frequency (RF) excitation in the ion cyclotron frequency range (ICRF) have been sustained in axisymmetric mirror cells and tandem mirrors.[7-9] The stability has been attributed to the effect of the radial RF ponderomotive force.[10,11]

Even when mirrors are MHD stable, they are subject to microinstabilities. Mirror-confined plasmas tend to have anisotropic, loss-cone velocity distributions except when they are highly collisional and flow [12] confined. In mirrors sustained by neutral beam injection, the drift-cyclotron loss-cone (DCLC) mode [13] and the Alfvén-ion cyclotron (AIC) mode [14,15] have been observed to limit energy confinement. These instabilities produce strong plasma fluctuations with frequencies $\omega \sim \omega_{ci}$ (ICRF regime). The interaction of the plasma with these fluctuations produces RF velocity-space diffusion which leads to a more stable velocity distribution. The DCLC mode has been successfully stabilized by a warm streaming plasma [13,14] but the AIC mode has been observed even when neutral beams are injected with mirroring points off of the midplane (so-called sloshing ions) to reduce anisotropy.[14,15] These instabilities are typically not seen in ICRF-sustained mirrors for two reasons. Energetic neutral injection produces plasmas with both higher anisotropy and $\beta_\perp$ (the ratio of the perpendicular plasma pressure to the magnetic field pressure), providing more drive for microinstability than ICRF-produced plasmas. Also, externally applied ICRF can provide RF diffusion in the same manner as the unstable mode.

This paper reports the stability properties of plasmas produced by ICRF in the central

cell of the Tara tandem mirror. The slow ion cyclotron wave was excited in a region where $\omega < \omega_{ci}$ and propagated along the magnetic field to resonances where $\omega = \omega_{ci}$. The wave propagation and heating characteristics of this experiment are described in a separate paper.[16] Other tandem mirrors have used fast wave heating with $\omega \gtrsim \omega_{ci}$ in the regions of excitation and heating, or non-resonant heating, with $\omega < \omega_{ci}$ everywhere in the central cell.[10,17]

The plasmas in the Tara central cell were maintained in a steady-state, stable, axisymmetric configuration by the ICRF alone. By stable is meant that no macroscopic (MHD-like) plasma motion was observed. The central cell also contained an axisymmetric magnetic divertor which supplemented the stability provided by the ICRF. The ICRF stabilization in the Tara central cell differs from other ICRF stabilization experiments since it was achieved by slow wave propagation into a magnetic beach. In a similar experiment in the Phaedrus tandem mirror, stabilization was achieved by slow wave excitation in a region of uniform magnetic field where $\omega < \omega_{ci}$.[18] The Tara magnetic geometry provided stabilization as well as strong ion heating at the ion cyclotron resonance.

The heating and fueling configuration in the Tara central cell produced hot ion plasmas with $\beta_\perp$ and anisotropy sufficient to produce microinstability. The observed unstable mode was strongest under the conditions where the heating was expected to be strongest and appeared to limit the peak $\beta_\perp$ that could be achieved.

The paper is organized as follows. The Tara configuration, parameters, and diagnostics are discussed briefly in Sec. II. They are discussed in more detail in Secs. II and III of Ref. 16. Section III of this paper presents the experimental results regarding macroscopic (MHD) stability of ICRF-produced plasmas. Section IV discusses calculations based on the ponderomotive stabilization model. Microstability will be discussed in Sec. V and conclusions are presented in Sec. VI.

II. DESCRIPTION OF THE EXPERIMENT

The Tara central cell was 10 meters in length, with the minimum field typically 2.2 kG, and the mirror ratio 11.5. In the midplane region the magnetic field was increased to

produce a "bump" of mirror ratio 1.8. The gas box for fueling and slot antenna for ICRF excitation were located on either side of the midplane on the bump.[8] An axisymmetric magnetic divertor was also located on the bump, between the ICRF antenna and the gas box. About 20-25% of the magnetic flux was mapped outside of the separatrix produced by the divertor. The divertor provided MHD stabilization which supplemented the stability provided by the ICRF. The divertor stabilization was not from pressure-weighted good curvature but rather from electron azimuthal mobility near the null magnetic field point.[6] This configuration is illustrated in Fig. 1.

By separating the region of high charge exchange losses associated with the gas fueling from the ICRF resonances which were located near the minimum field regions or "wells" on either side of the bump, hot mirror-confined ions were produced in the wells. The application of 250-500 kW of ICRF at 3.47 MHz produced plasmas in the wells with 400-800 eV ions, 75-100 eV electrons, densities of $3 - 5 \times 10^{12}$ cm^{-3}, and peak $\beta_\perp$ of 2-3%. The radial density profile had a Gaussian form with a scale length of 1/2 - 2/3 the limiter radius of 20 cm.[16]

The central cell was bounded on each side by axisymmetric plug cells outboard of which the plasma was mapped through quadrupole mirror cells. The quadrupole mirrors could provide MHD stability when their good curvature was weighted by sufficient plasma pressure by local ICRF heating.[19] For the experiments described in this paper, no ICRF was provided in the quadrupole cells so they played no role in MHD stability. It is for this reason that the configuration is described as axisymmetric. The results presented here are for unplugged operation, with no ion confining potentials being produced in the plug cells.

The principal diagnostics used to characterize the plasma were arrays of diamagnetic loops for stored energy and anisotropy, arrays of microwave interferometers for axial and radial density profiles, and arrays of biasable particle collectors at the end walls to measure end loss profiles. The fluctuations associated with macroscopic instability were observed on interferometers, end loss collectors, and arrays of plasma light detectors.[20] Fluctuations associated with microstability were observed on an array of radially movable RF magnetic probes and a microwave scattering diagnostic.[21] The diagnostics are discussed in more

detail in Ref. 16.

III. MHD STABILIZATION BY ICRF

A stable plasma was produced in the central cell by ICRF with no stabilizing $\beta_\perp$ in the quadrupole cells and without the magnetic divertor in the central cell. Since axisymmetric mirrors are unstable to curvature-driven modes according to MHD theory, a stabilization mechanism must have been operative during these experiments. The stability of the plasma was sensitive to the ICRF power, the gas fueling rate, the resonance location, and the magnetic field of the bump. When the plasma was unstable, the MHD mode observed was radially rigid and flute-like, with an azimuthal mode number $m = 1$. It typically grew to a large amplitude, saturated state where the entire plasma column was displaced from the magnetic axis by 4-8 cm and rotated about the magnetic axis at a frequency of 5-20 kHz.[20]

ICRF stabilization of this mode is illustrated in Fig. 2. Here an unstable plasma was produced at a relatively low ICRF power of 250 kW, in this case by using a very low gas fueling rate. The instability is seen as a fluctuation on the central chord line density and a displacement and oscillation of the plasma light centroid (position of the peak from a Gaussian fit to data from the radial array of plasma light detectors). From 15-25 ms the ICRF power was doubled, during which time the plasma fluctuations were eliminated and the plasma density and $\beta_\perp$ built up. Improved stability was in general determined by the observation of lower plasma fluctuation levels, as seen in Fig. 2 . There was typically an abrupt threshold for instability, rather than a gradual increase in fluctuation level. Improved ambipolar radial confinement was associated with lower fluctuation levels. This was seen in the ratio of the total end loss current to the fueling current. Lower fluctuations correlated with an increase in this ratio. Instability could be produced in a number of ways, as will be discussed later, and in all cases increasing the ICRF power improved stability. When destabilizing $\beta_\perp$ was produced in the plug cells (by ICRF or electron cyclotron heating), higher central cell ICRF power allowed more plug $\beta_\perp$ to be supported before instability resulted.

The stability properties of the ICRF increased faster with power than the instability

drive produced by the heating. The stored energy in the plasma was shown to saturate at high ICRF power[16] while the stabilization always increased with power. The edge plasma density decreased with increasing power[16] , making it unlikely that the stabilization was due to edge line tying. The other sources of stability, the divertor and the quadrupole cells, were shown to provide stabilization which was additive with the ICRF stabilization.[6,19]

The gas fueling rate played a very important role in the stability of the plasma. For a fixed ICRF power, the plasma became unstable when the fueling rate was too low or too high. At low fueling rate, the instability had the steady-state character shown in Fig. 2 . The plasma radius decreased when the fueling rate was lowered and this was shown to reduce the ICRF coupling.[16] Changes in the plasma radial profile that affect the ICRF fields change both the power deposition and stabilization profiles. The ponderomotive model for ICRF stabilization (which is discussed in the next section) depends on the radial profiles of the RF electric fields. The radial equilibrium is established by a balance of the radial profiles of the fueling and heating with the particle and power loss profiles. A stable equilibrium also requires a balance of the instability drive with the stabilization, which are both produced by the ICRF in this case. A stable equilibrium was not achievable at low gas fueling rates.

At very high fueling rates, a relaxation oscillation occurred with a period of several milliseconds. Each drop in density and diamagnetism was accompanied by a burst of $m = 1$ fluctuations. When the ICRF power was raised the stabilization was increased relative to the heating and the relaxation oscillation was eliminated. The window for stable operation was not restrictive and the addition of the divertor allowed an even wider range of stable operation (typically 15-30 Torr-liters/sec).

MHD stability was sensitive to the location of the ICRF resonance. For a given gas fueling rate and ICRF power, the plasma had an abrupt threshold to instability when the resonance was moved up the gradient from the magnetic well minimum field on either side of the midplane bump. This is illustrated in Fig. 3 where the fluctuation amplitude of the line density is plotted vs. the mirror ratio at the resonance location, R_m. R_m is equivalent to ω/ω_{ci_0}, where ω_{ci_0} is the ion cyclotron frequency at the magnetic well minimum field.

These data were produced by varying only the minimum field in the central cell while keeping the ICRF frequency and the bump field fixed, so that the antenna coupling was not perturbed. Data is shown for two cases, with and without the divertor. Without the divertor, there was an abrupt change in fluctuation amplitude at R_m=1.06, when a strong $m = 1$ mode was generated. The plasma density and $\beta_\perp$ showed a large drop associated with the instability. Data for only one unstable value of R_m is shown because above the threshold it was not possible to produce a plasma. With the divertor, the threshold is increased to R_m=1.09. It was also possible to maintain stability at a lower gas fueling rate with the divertor. Figure 3 shows stability thresholds for two particular cases. The threshold for optimized conditions of divertor, gas, and power was R_m=1.15.

An explanation of this behavior relies on two effects. They are that destabilizing field line curvature increases with mirror ratio and, as will be discussed in the section on microstability, that the axial extent of the hot ions in the wells was governed by the resonance location. Moving the resonance to higher mirror ratio produced more plasma pressure in the regions of the central cell with bad curvature, eventually leading to instability. Increasing the ICRF power raised the resonance mirror ratio at which the instability threshold occurred. At a given ICRF power, the effect of operating the divertor was to allow stable operation with the resonance at a higher mirror ratio.

The stability properties of the ICRF were also affected by the bump magnetic field. This is shown by varying the bump field with the well field held fixed. In Fig. 4, the fluctuation amplitude of the line density is plotted vs. the bump-to-well mirror ratio R_b, which is approximately equal to ω/ω_{ci} at the antenna. There was a threshold for instability when R_b was increased to the point that ω/ω_{ci} at the antenna was below 0.55. The resonance location was not significantly changed by varying the bump field, with any small change caused by increasing the bump field moving it to a lower and more stable mirror ratio. The effect of the divertor was again to allow stable operation at higher bump fields than without the divertor.

This threshold appears to be due to a change in the ICRF stabilization rather than the MHD drive. Changing ω/ω_{ci} at the antenna location by varying the bump field affects

the coupling to the slow wave. Since the wave field radial profiles were observed to be roughly preserved as the ICRF propagated along the magnetic field gradient[16] , changes in the profiles at the point of excitation would likely affect the overall stabilization properties. Varying the bump field might also affect the coupling by changing the density at the bump, but access to measure this was not available.

Another possible explanation concerns the effect of mode conversion at the Alfvén resonance.[22] For the conditions in the Tara central cell, the Alfvén resonance occurred near the edge of the plasma and moved into the plasma as the bump magnetic field was increased or the density was decreased. There was no experimental evidence to elucidate the role played by the Alfvén resonance.

IV. PONDEROMOTIVE STABILIZATION CALCULATIONS

The stabilization of MHD instabilities by ICRF has been attributed to the action of the ponderomotive force.[9-11] The stabilizing force is produced by the radial gradients of the RF electric fields. In the ICRF regime the ponderomotive force may be written as [23]

$$F_p = \frac{-e^2}{4m_i}\left[\frac{\nabla_r E_+^2}{\omega_{ci}(\omega-\omega_{ci})} - \frac{\nabla_r E_-^2}{\omega_{ci}(\omega+\omega_{ci})} + \frac{m_i}{m_e}\frac{\nabla_r E_z^2}{\omega^2}\right]. \quad (1)$$

Since the RF electric field radial profiles are not directly measured, it is necessary to use models to calculate of the stabilizing force. The McVey code has typically been used to model ICRF heating and stabilization in mirror geometry.[17,23,24] The code includes the antenna geometry in detail, stratifed radial profiles of plasma parameters, Doppler-shifted ion cyclotron damping, and electron Landau damping. It does not include the effects of axial gradients, most importantly, the magnetic field gradient.

For the Tara case, the code is run using the magnetic field at the antenna location in order to model the coupling correctly, but the ion absorption is therefore incorrect. The code predictions for RF magnetic field radial profiles have been compared to experimentally measured profiles. For the range of 130-190 cm from the antenna, where experimental data is available, they agree reasonably well in form and magnitude for the inner 2/3 of the profile. An example is shown in Fig. 5 for 195 cm from the antenna. The disagreement

at the plasma edge is due to the strong edge fields predicted by the code from the $m = 1$ fast wave.[23,25] This mode is apparently not excited in the experiment, perhaps because of the close proximity of axial gradients, particularly those of the divertor, to the antenna. The good agreement between the code and experiment would not be expected very close to the resonance but experimental measurements were done only up to 195 cm from the antenna where ω/ω_{ci}=0.87. The measured parallel wave number, $k_{\|}$, also agreed with the code. More detail on how the code was applied to this experiment may be found in Ref. 16.

Since there was reasonable agreement between the measured and calculated RF magnetic field profiles, the RF electric field profiles from the McVey code have been used in Eq. (1) to gain some insight into the stabilization. The result is shown in Fig. 6 . In this figure the pondermotive force has been averaged azimuthally for the axial position 130 cm from the antenna. One clear observation is that contribution of the E_+ term to the ponderomotive force dominates over the entire profile. This is true at all axial positions. The force is stabilizing over roughly the middle third of the plasma and is strongly destabilizing in the outer third. Since the edge fields were not observed in the experiment, their destabilizing effect would also be absent.

The stabilizing region inside the plasma is due to a region of negative slope in the E_+ profile, as is required in Eq. (1) when $\omega < \omega_{ci}$. Figure 7 shows an r-θ surface plot of E_+ from McVey code results for 130 cm from the antenna. The region of negative (stabilizing) slope exists at all azimuthal angles. The large, destabilizing edge fields can be seen but these were not observed in the experimental measurements. The existence of a stabilizing region is sensitive to the distance from the antenna, the radial density profile, and ω/ω_{ci}. The stabilizing region is not predicted by the code at axial positions less than 90 cm from the antenna and there is more radial structure and weaker stabilization for distances greater than 160 cm from the antenna. An axial average of the ponderomotive force is dominated by the near field contribution and is net destabilizing. This is not consistent with the observed stabilization and implies that the code does not accurately model the experiment. The close proximity of the divertor to the antenna likely played an

important role in determining the near fields of the antenna. Even when the divertor coil is turned off, it is necessary to produce very strong gradients near the antenna to map the flux through this region.[6]

Figures 6 and 7 are from calculations with $\omega/\omega_{ci} = 0.65$ and a Gaussian radial scale length $r_p = 13$ cm; values which are consistent with the best experimental conditions. When r_p is decreased to 10 cm or increased to 19 cm, the region of stabilizing slope is reduced significantly. For the $r_p = 13$ cm case, lowering ω/ω_{ci} below 0.55 eliminates the stabilizing region. With the limitations on the applicability of the model in mind, these predictions do show qualitative agreement with experimental observations. In the experiment, MHD stability was lost for very high and very low gas fueling rates, corresponding to the very broad and very narrow density profiles that are predicted not to be less stabilizing. The loss of the stabilizing region for lower ω/ω_{ci} agrees with the experimental result that MHD stability was lost when the bump field was raised (see Fig. 4).

V. MICROSTABILITY

When the applied ICRF was resonant near the magnetic well minimum field, a plasma-generated mode was observed by RF magnetic probes and by the microwave scattering diagnostic[21] located in the north plug cell. A similar mode was also observed during ICRF heating in the norh plug cell.[21] Frequency spectra from a magnetic probe for two central cell resonance locations are shown in Fig. 8. In the lower spectrum, two large frequency peaks are seen, one the applied ICRF at 3.47 MHz and another close to, but below, both the applied ICRF frequency and ω_{ci} at the well midplane, ω_{ci_0}. The second peak split into as many as three closely spaced peaks when it was excited most strongly, as shown in the upper spectrum in Fig. 8. The plasma-generated mode was stronger when the ion cyclotron resonance was closer to the well midplane.

Figure 9 shows the scaling of the frequency of the mode with the resonance mirror ratio of the applied ICRF, R_m. For a fixed applied ICRF frequency, R_m was varied by changing the magnetic field in the wells. The magnetic field of the bump was held fixed so that the coupling would not be affected. It can be seen that the frequency of the plasma-generated

mode was 0.8-0.9 ω_{ci_0}, tracking the variation of the well field. The mode amplitude was strongly dependent on R_m. This point will be discussed later.

Axially spaced magnetic probes provided data on the wavelength of the mode. The probes were located along the magnetic field gradient between the bump and the north well, measuring the fluctuating magnetic fields in the range $0.65 \lesssim \omega/\omega_{ci} \lesssim 0.9$. The probe data were analyzed using digital spectral analysis techniques.[26,27] Figure 10 shows the scaling of the axial wave number, k_z, with ω/ω_{ci} for the plasma-generated mode. Here B_θ data were used and the value of ω/ω_{ci} is the average of the locations of the two probes used to determine k_z. The magnitude and scaling of k_z agrees reasonably well with the dispersion relation for the cold plasma ion cyclotron wave, shown as a solid line in the figure. The cold plasma result plotted here is for a fixed, representative density of $1 \times 10^{12} cm^{-3}$, while there was some variation in the density over the range of the experimental conditions. Much of the scatter in the experimental data was due to the difficulty of the measurement under many of the conditions because the mode was only weakly excited. A radial profile of the B_θ component of the mode is shown in Fig. 11 for the case where $R_m = 1.03$. The mode amplitude was small at the edge and peaked at about 6 cm from the axis. The point at 3 cm may be lower because the probe perturbs the plasma at this location, reducing $\beta_\perp$. The mode is seen to have been strongest in the high $\beta_\perp$ core plasma.

These results indicate that the instability was the AIC mode. The AIC instability is an electromagnetic instability that propagates primarily along the magnetic field.[28] The DCLC instability produces an electrostatic mode with small k_z[13], which is not at all consistent with the data. The AIC instability occurs in plasmas with high ion $\beta_\perp$ and anisotropic ion velocity distributions. It has been observed in mirror cells driven by perpendicular and angled neutral beam injection and was shown to degrade ion confinement.[14,15] An instability beta limit has been derived for an ion distribution that uniformly fills the confined velocity space of a mirror.[28] This is a reasonable model of the ICRF-heated Tara central cell where the ion cyclotron resonance position defined a hot ion plasma length which filled the two well mirrors roughly uniformly out to the mirror ratio of the resonance, R_m. The

beta limit is

$$\beta_\perp = 3.52\ (T_\parallel/T_\perp)^2, \qquad T_\parallel/T_\perp \ll 1\ . \tag{2}$$

The limit is lower when the anisotropy, defined as the ratio of the perpendicular to parallel ion temperatures ($T_\perp/T_\parallel$), is higher. The presence of a warm ion component (the passing ions which are trapped in the central cell but not in one of the wells) raises the beta limit for a given anisotropy. For the Tara central cell the correction to Eq. (2) is 10-20% (from Eq. 28 of Ref. 28).

Figure 12 shows the experimental scaling of $\beta_\perp$, the anisotropy, and the AIC amplitude when R_m was varied. The anisotropy, defined here as the ratio of the perpendicular to parallel plasma pressure, was determined from two axially spaced diamagnetic loops in the well.[29] The data shown are for the south well which typically had 2-3 times higher $\beta_\perp$ than the north because of the asymmetric location of the gas box on the bump.[16] Each data point is the average of several shots at the same conditions. Also shown is the drive term, $\beta_\perp \times (T_\perp/T_\parallel)^2$, assuming $p_\perp/p_\parallel = T_\perp/T_\parallel$. From Eq. (2) , values greater than 3.52 should be unstable. For the data represented by triangles, $\beta_\perp$ was the peak value assuming the peaking effect of the measured density profile. The drive was clearly highest when the instability was observed to be strongest (when the resonance was closest to the well midplane) but the drive was lower than the predicted threshold. Though there was no experimental measurement of the ion temperature profile, there was some indirect experimental information based on the measured density, neutral hydrogen, and charge exchange profiles. The self-consistency of these measured profiles requires that the ion temperature be peaked on axis in a similar manner to the density.[30] This would increase the instability drive by a factor of four (as shown by the data represented by circles in Fig. 12), making the results consistent with the simple model being applied here.

The heating was expected to be strongest when the resonance was closest to the well minimum field region since the resonant interaction between the ions and the ICRF would occur over the longest distance. The hot mirror-trapped ions produced by the heating tend to localize between the midplane of the well mirror and the resonance[31] making the anisotropy depend on resonance location. The data in Fig. 12 show that the highest

$\beta_\perp$ was not achieved with the resonance at the well minimum field. It appears that the AIC instability was limiting the effectiveness of ICRF heating when it was expected to be strongest due to the highly anisotropic mirror-trapped hot ions that were produced. The effect of the unstable AIC mode is to reduce the anisotropy through the resonant interaction between the ion parallel motion and unstable wave when $(\omega - \omega_{ci}) = k_\parallel v_\parallel$. By increasing the ion parallel velocity, $v_\parallel$, the instability degrades mirror confinement.

V. CONCLUSIONS

The ICRF experiments in the central cell of the Tara tandem mirror demonstrated that slow wave propagation into a magnetic beach provides MHD stability as well as effective heating. The ICRF stabilization allowed operation in an axisymmetric configuration without high beta plasma in the quadrupole mirror cells. The stability provided by the combination of ICRF and the divertor was sufficiently robust to maintain stability even when destabilizing $\beta_\perp$ was built up in the axisymmetric plug cells during end plugging experiments.[6]

The maintenance of MHD stability put limitations on the operating regime of the experiment. Increasing the mirror ratio of the bump would be advantageous for energy confinement by reducing charge exchange losses from the hot miror-trapped ions in the wells.[8] MHD stability required that the resonance be kept close to the well minimum field and that ω/ω_{ci} on the bump be sufficiently high, limiting the bump mirror ratio to less than two. Lowering the gas fueling rate reduces both charge exchange losses and radiation losses from electrons, but also led to MHD instability.

The RF ponderomotive force provides a consistent explanation of the observed ICRF stabilization. McVey code results show that when the edge fast wave contribution is neglected, stabilizing RF electric field profiles are predicted when sufficiently far from the antenna. For the range of distance from the antenna where stabilizing profiles are predicted, there was reasonable agreement between the code and experimentally measured profiles except near the plasma edge. The absence of the edge fast wave fields in the experimental measurements justifies neglecting their effect in the model calculation. The

stabilizing region predicted by the code should therefore have existed in the experiment.

The strongly destabilizing code predictions from the antenna near fields caused overall disagreement between the code and the experiment. However, there is good reason to expect that the near fields are not well modelled by the code due to the strong magnetic field gradients in the divertor region next to the antenna.

Another clear result of the code calculations was the dominance of the E_+ contribution to the radial pondermotive force at all radii and under all conditions that were studied. The code predicted stabilizing fields only in the central region of the plasma. The narrow Gaussian radial profile of the slow-wave-produced plasmas in Tara may have been due, at least in part, to the ponderomotive stabilization profile. A stable equilibrium may have only been attainable for narrow plasma profiles. The existence of the stabilizing region was sensitive to the density profile and ω/ω_{ci} in a manner which would explain the stability boundaries observed in the experiment. This gives more credence to the ponderomotive force as the stabilization mechanism.

MHD stable hot ion plasmas were produced by the externally excited slow wave but there was insufficient collisional and RF velocity-space diffusion to limit the anisotropy produced by the heating. The AIC instability, which channels plasma energy into a slow wave, occurred even when the heating source for the plasma was also a slow wave. To limit the ion anisotropy and maintain microstability, the resonance could not be too close to the well minimum field. There was a range of resonance mirror ratio of roughly 1.05-1.15 over which both MHD stability and microstability could be maintained.

The improved confinement provided by end plugging would influence stability. The experiments descibed here were performed in the absence of significant end plugging. If strong end plugging were present in a tandem mirror, microstability would be expected to improve. End plugging confines loss-cone ions, making the central cell plasma more isotropic. Additionally, lower gas fueling would be required to maintain the density, reducing the charge exchange rate and allowing the hot ions to undergo more pitch angle scattering before being lost. This would further reduce the anisotropy.

On the other hand, the more axially uniform plasma in a plugged central cell would put more plasma pressure in bad curvature regions, increasing the drive for MHD instability. Additional divertors or ICRF antennas on the gradients at each end of the central cell could be used to provide additional stabilization while preserving axisymmetry.

ACKNOWLEDGEMENTS

It is a pleasure to acknowledge the support of the Tara tandem mirror engineering and technical staff whose work contributed greatly to the attainment of these results.

This work was supported by U. S. Department of Energy Contract No. DOE-AC02-78ET51013.

References

[1]Y. B. Gott, M. C. Ioffe, and V. G. Telkovsky, in *Proceedings of the Conference on Plasma Physics and Controlled Nuclear Fusion Research, Salzburg, 1961* (International Atomic Energy Agency, Vienna, 1963), Part 3, p. 1045.

[2]A. W. Molvik, R. A. Breun, S. N. Golovato, N. Hershkowitz, B. McVey, D. Smatlak, and L. Yujiri, *Phys. Rev. Lett.* **48**, 742 (1982).

[3]R. P. Drake, E. B. Hooper, Jr., C. V. Karmendy, S. L. Allen, T. A. Casper, J. F. Clauser, F. H. Coensgen, R. H. Cohen, D. L. Correll, J. C. Davis, J. H. Foote, A. H. Futch, R. K. Goodman, D. P. Grubb, G. E. Gryczkowski, G. A. Hallock, A. L. Hunt, W. E. Nexsen, W. L. Pickles, A. E. Pontau, P. Poulsen, T. C. Simonen, O. T. Strand, and W. R. Wampler, *Phys. Fluids* **25**, 2110 (1982).

[4]D. K. Smith, K. Brau, P. Goodrich, J. Irby, M. E. Mauel, B. D. McVey, R. S. Post, E. Sevillano, and J. Sullivan, *Phys. Fluids* **29**, 902 (1986).

[5]J. R. Ferron, A. Y. Wong, G. Dimonte, and B.J. Leikind, *Phys. Fluids* **26**, 2227 (1983).

[6]J. A. Casey, B. G. Lane, J. H. Irby, K. L. Brau, S. N. Golovato, W. C. Guss, J. Kesner, R. S. Post, E. Sevillano, and J. Zielinski, MIT Report PFC/JA-87-25 (submitted to *Phys. Fluids*).

[7]R. Breun, S. N. Golovato, L. Yujiri, B. McVey, A. Molvik, D. Smatlak, R. S. Post, D. K. Smith, and N. Hershkowitz, *Phys. Rev. Lett.* **47**, 1833 (1981).

[8]R.S. Post, K. Brau, S. Golovato, E. Sevillano, D.K. Smith, W. Guss, J. Irby, R. Myer, and J. Sullivan, *Nuclear Fusion* **27**, 217 (1987).

[9]Y. Yasaka and R. Itatani, *Nuclear Fusion* **24**, 445 (1984).

[10]J. R. Ferron, N. Hershkowitz, R. A. Breun, S. N. Golovato, and R. Goulding, *Phys. Rev. Lett.* **51**, 1955 (1983).

[11]J.R. Myra and D.A. D'Ippolito, *Phys. Rev. Lett.* **53**, 914 (1984).

[12]T. D. Rognlien and T. A. Cutler, *Nuclear Fusion* **20**, 1003 (1980).

[13]W. C. Turner, E. J. Powers, and T. C. Simonen, *Phys. Rev. Lett.* **39**, 1087 (1977).

[14]T. A. Casper and G. R. Smith, *Phys. Rev. Lett.* **48**, 1015 (1982).

[15]L. V. Berzins and T. A. Casper, *Phys. Rev. Lett.* **59**, 1428 (1987).

[16]S. N. Golovato, K. Brau, J. Casey, J. Coleman, M. J. Gerver, W. Guss, G. Hallock, S. Horne, J. Irby, R. Kumazawa,J. Kesner, B. Lane, J. Machuzak, T. Moran, R. Myer, R. S. Post, E. Sevillano, D. K. Smith, J. D. Sullivan, R. Torti, L. Wang, Y. Yasaka, X.Z. Yao, and J. Zielinski, MIT Report PFC/JA-88-15 (submitted to *Phys. Fluids*).

[17]G. Dimonte, A. W. Molvik, J. Barter, W. F. Cummins, S. Falabella, P. Poulsen, and T. Romesser, *Nuclear Fusion* **27**, 1959 (1988).

[18]J. J. Browning, R. Majeski, T. Intrator, N. Hershkowitz, and S. Meassick, *Phys. Fluids* **31**, 714 (1988).

[19]K. Brau, B. Lane, J. Casey, S. Horne, J. Kesner, S. N. Golovato, J. H. Irby, R. S. Post, E. Sevillano, and D. K. Smith, *Nuclear Fusion* (to be published).

[20]J.H. Irby, B.G. Lane, J.A. Casey, K. Brau, S.N. Golovato, W.C. Guss, S.F. Horne, J. Kesner, R.S. Post, E. Sevillano, J.D. Sullivan, and D.K. Smith, *Phys. Fluids* **31**, 902 (1988).

[21]J. S. Machuzak, P. Woskoboinikow, W. J. Mulligan, D. R. Cohn, M. Gerver, W. Guss, M. Mauel, R. S. Post, and R. J. Temkin, *Rev. Sci. Instrum.* **57**, 1983 (1986).

[22]J. R. Myra, private communication.

[23]J. R. Ferron, S. N. Golovato, N. Hershkowitz, and R. H. Goulding, *Phys. Fluids* **30**, 1869 (1987).

[24]See National Technical Information Service Document No. DE85004960 ("ICRF An-

tenna Coupling Theory for Cylindrically Stratified Plasma," Massachusetts Institute of Technology Report PFC/RR-84-12 by B. McVey). Copies may be ordered from the National Technical Information Service, Springfield, Virginia 22161. The price is $16.95 plus a $3.00 handling fee. All orders must be prepaid.

[25]F. J. Paoloni, *Phys. Fluids* **18**, 649 (1975).

[26]D. E. Smith, E. J. Powers, and G. S. Caldwell, *IEEE Trans. Plasma Sci.* **PS-2**, 263 (1974).

[27]L. Wang, S. N. Golovato, and S. F. Horne, private communication (MIT Report No. PFC/RR-88-3).

[28]Gary R. Smith, *Phys. Fluids* **27**, 1499 (1984).

[29]J. Kesner, private communication.

[30]W. C. Guss, X. Z. Yao, L. Pócs, R. Mahon, J. Casey, S. Horne, B. Lane, R. S. Post, and R. P. Torti, *Phys. Fluids* (submitted for publication).

[31]S. N. Golovato, R. A. Breun, J. R. Ferron, R. H. Goulding, N. Hershkowitz, S. F. Horne, and L. Yujiri, *Phys. Fluids* **28**, 734 (1985).

Figure Captions

Figure 1. The Tara magnetic flux geometry showing the bump region, one of the central cell wells, and one axisymmetric end cell

Figure 2. The time evolution for the first 40 ms of a plasma shot in which the gas fueling was sufficiently low to produce a large $m = 1$ motion of the plasma. From 15-25 ms the ICRF power was doubled, resulting in the elimination of the macroscopic plasma motion.

Figure 3. The variation of the fluctuation amplitude on the central chord line density signal (the standard deviation divided by the mean over a 5 ms period) when the ion cyclotron resonance location was varied by changing only the magnetic well minimum field. The upper plot is for operation at a gas fueling rate of 20 Torr-liters/sec with the divertor. The lower plot is for operation at 26 Torr-liters/sec without the divertor.

Figure 4. The variation of the fluctuation amplitude on the central chord line density signal when the bump magnetic field, and therefore ω/ω_{ci} at the antenna location, was varied.

Figure 5. A comparison of B_θ radial profiles 195 cm from the antenna with experimental measurements shown as diamonds and McVey code results as a solid line. ω/ω_{ci}=0.87 for the measurements while the code results are for ω/ω_{ci}=0.65, the value at the antenna location.

Figure 6. Radial profiles of the ponderomotive force calculated from Eq. (1) using McVey code results for the RF electric fields. Plotted is the azimuthal average for a 13 cm Gaussian density profile 130 cm from the antenna.

Figure 7. A surface plot of McVey code results for the magnitude of E_+ in an r-θ plane 130 cm from the antenna, the same conditions as the results shown in Fig. 6.

Figure 8. Frequency spectra for two magnetic well minimum fields, corresponding to two ICRF resonance positions. The largest peak in each spectrum is the applied ICRF at 3.47 MHz.

Figure 9. The variation of the frequency of the plasma-generated mode when the magnetic well minimum field, and therefore the resonance location, was varied.

Figure 10. The scaling of the axial wave number, k_z, with ω/ω_{ci} for the plasma-generated mode. The experimentally measured points are shown as triangles and the cold plasma theory for a density of $1 \times 10^{12} cm^{-3}$ as a solid line

Figure 11. The amplitude of the plasma-generated mode as a function of radius, as measured by an RF magnetic probe.

Figure 12. The scaling of the measured instability drive and instability amplitude when the magnetic well minimum field was varied. The data shown as circles are a factor of four higher, assuming the peaking effect of the ion temperature profile as well as the density.

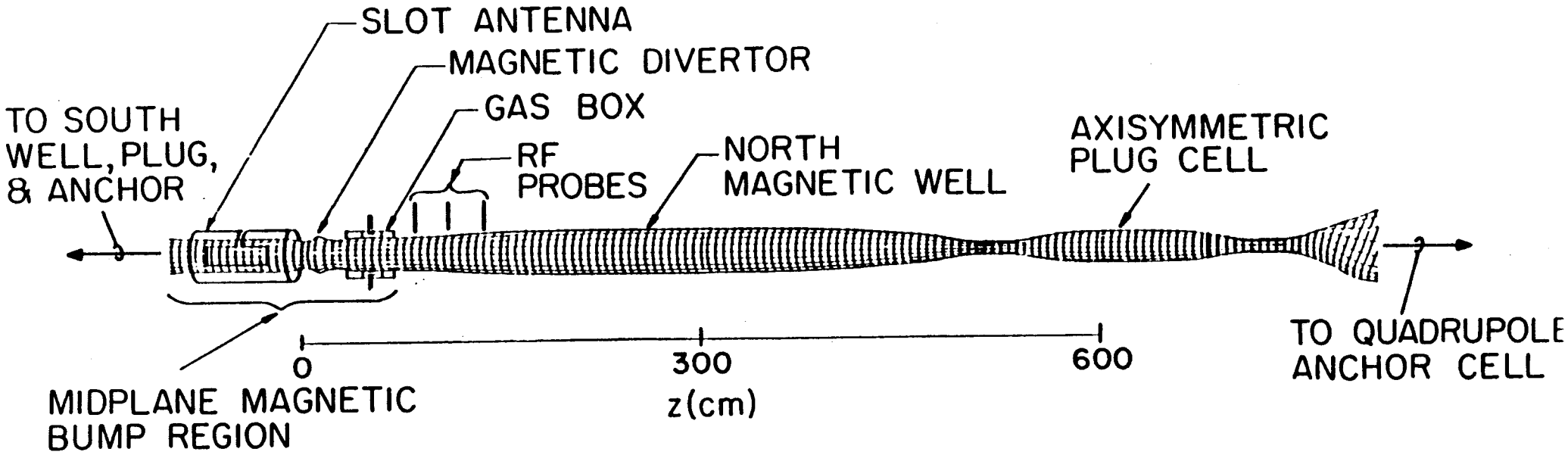

TARA MAGNETIC FLUX TUBE

Figure 1

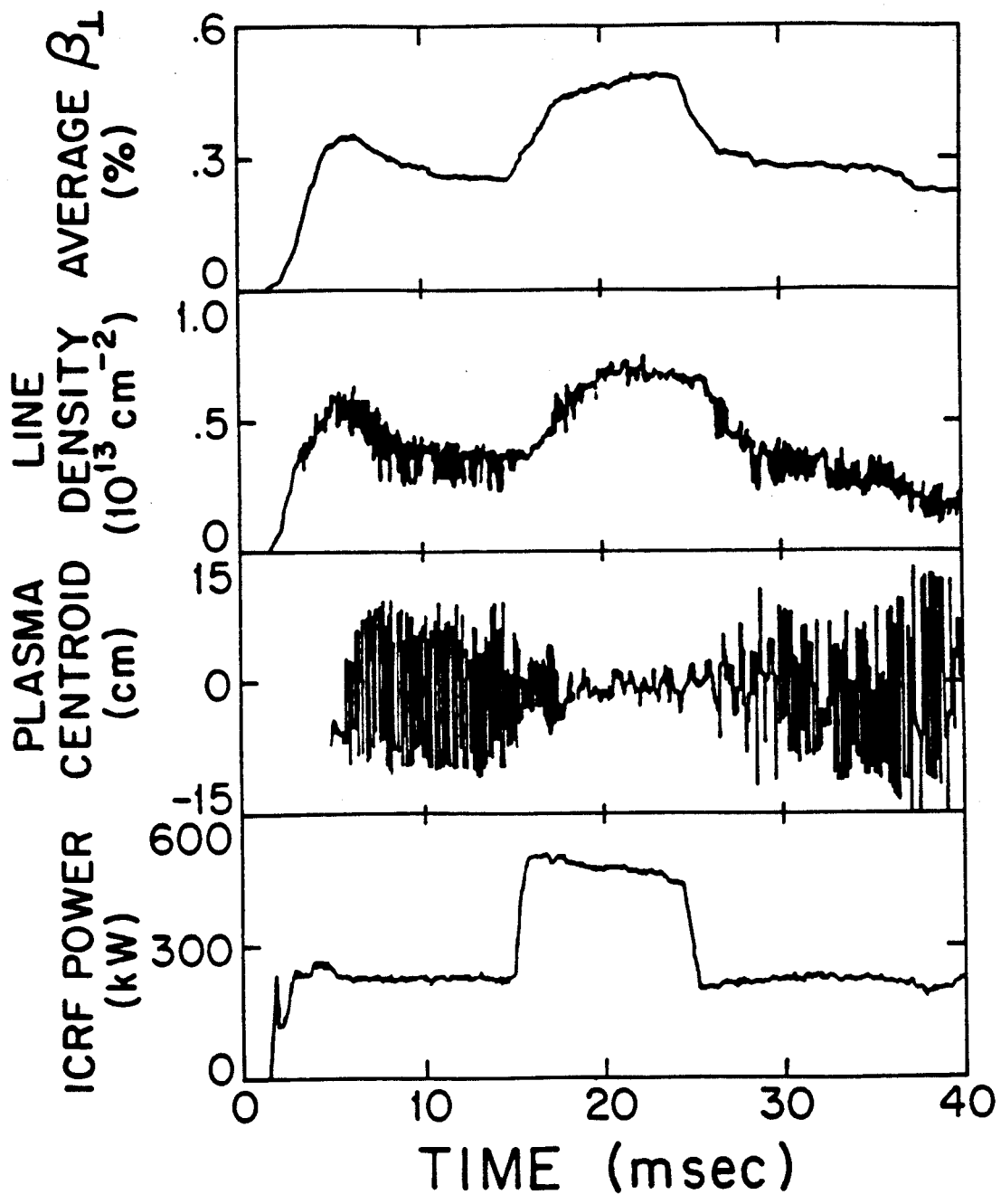
AVERAGE $\beta_\perp$ (%)
.6
.3
0
LINE DENSITY (10^{13} cm^{-2})
1.0
.5
0
PLASMA CENTROID (cm)
15
0
-15
ICRF POWER (kW)
600
300
0
0
10
20
30
40
TIME (msec)

Figure 2

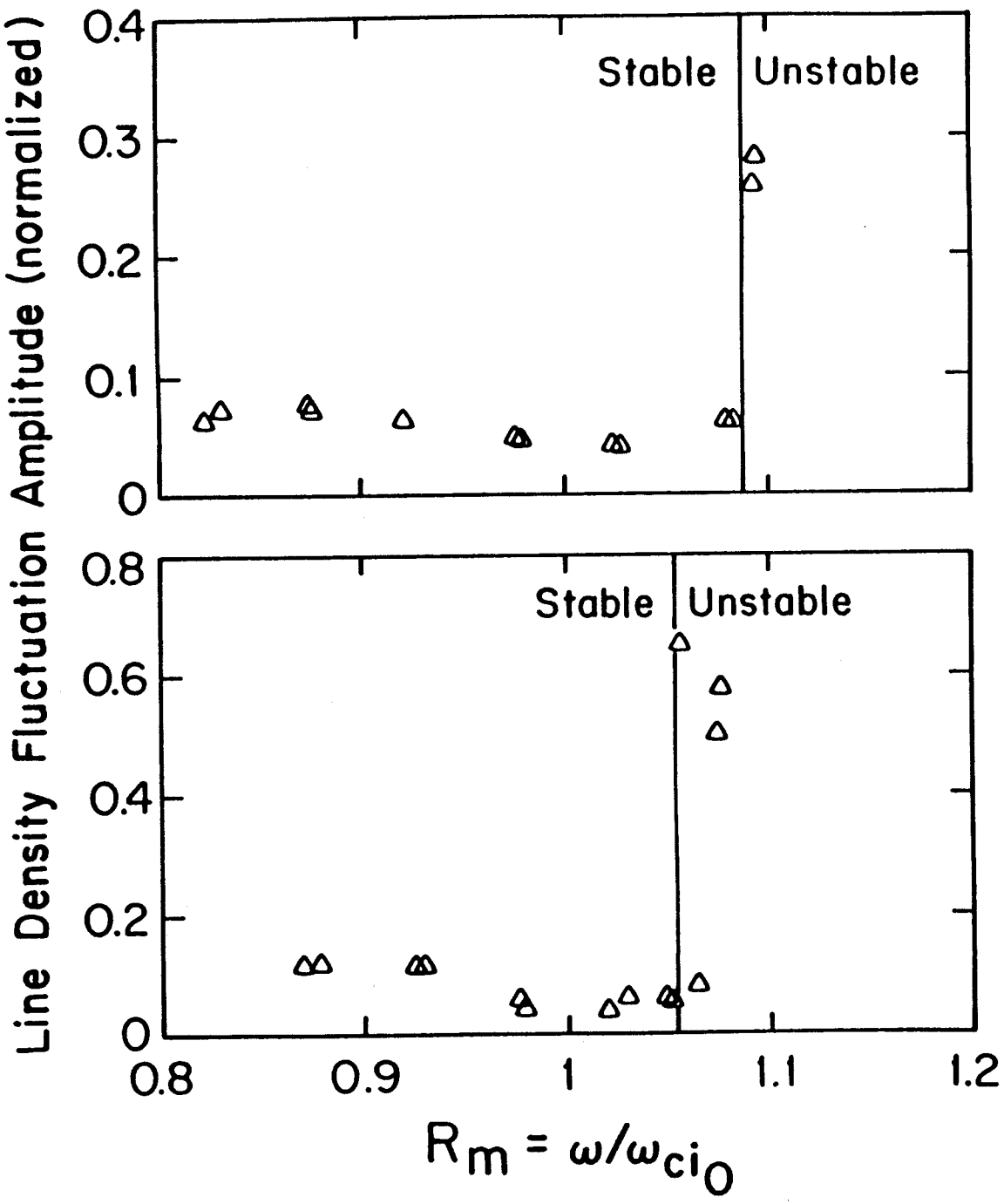
Line Density Fluctuation Amplitude (normalized)
0.4
0.3
0.2
0.1
0
Stable
Unstable
0.8
0.6
0.4
0.2
0
Stable
Unstable
0.8
0.9
1
1.1
1.2
$R_m = \omega/\omega_{ci_0}$

Figure 3

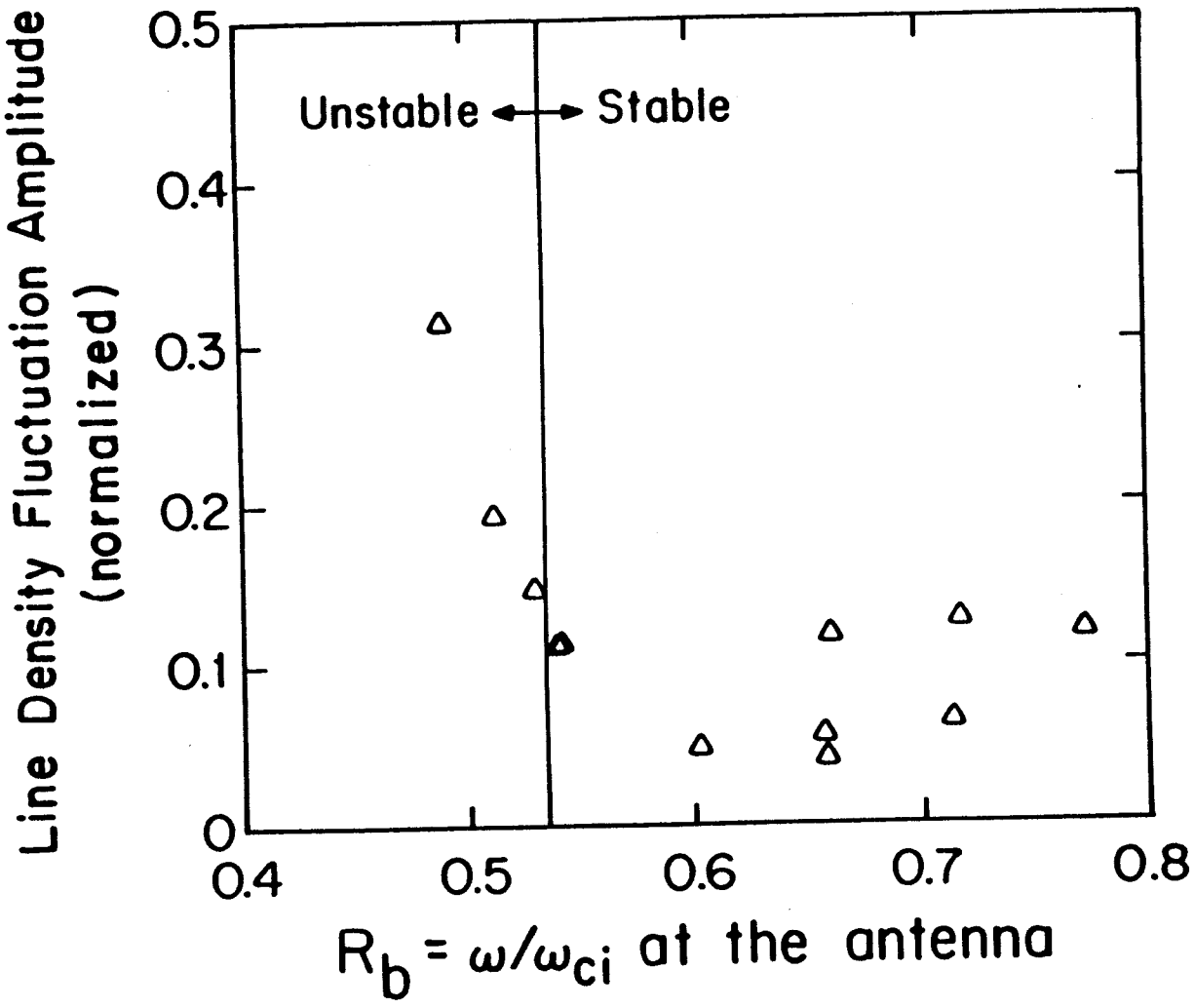
Line Density Fluctuation Amplitude
(normalized)
0.5
0.4
0.3
0.2
0.1
0
Unstable
Stable
0.4
0.5
0.6
0.7
0.8
$R_b = \omega/\omega_{ci}$ at the antenna

Figure 4

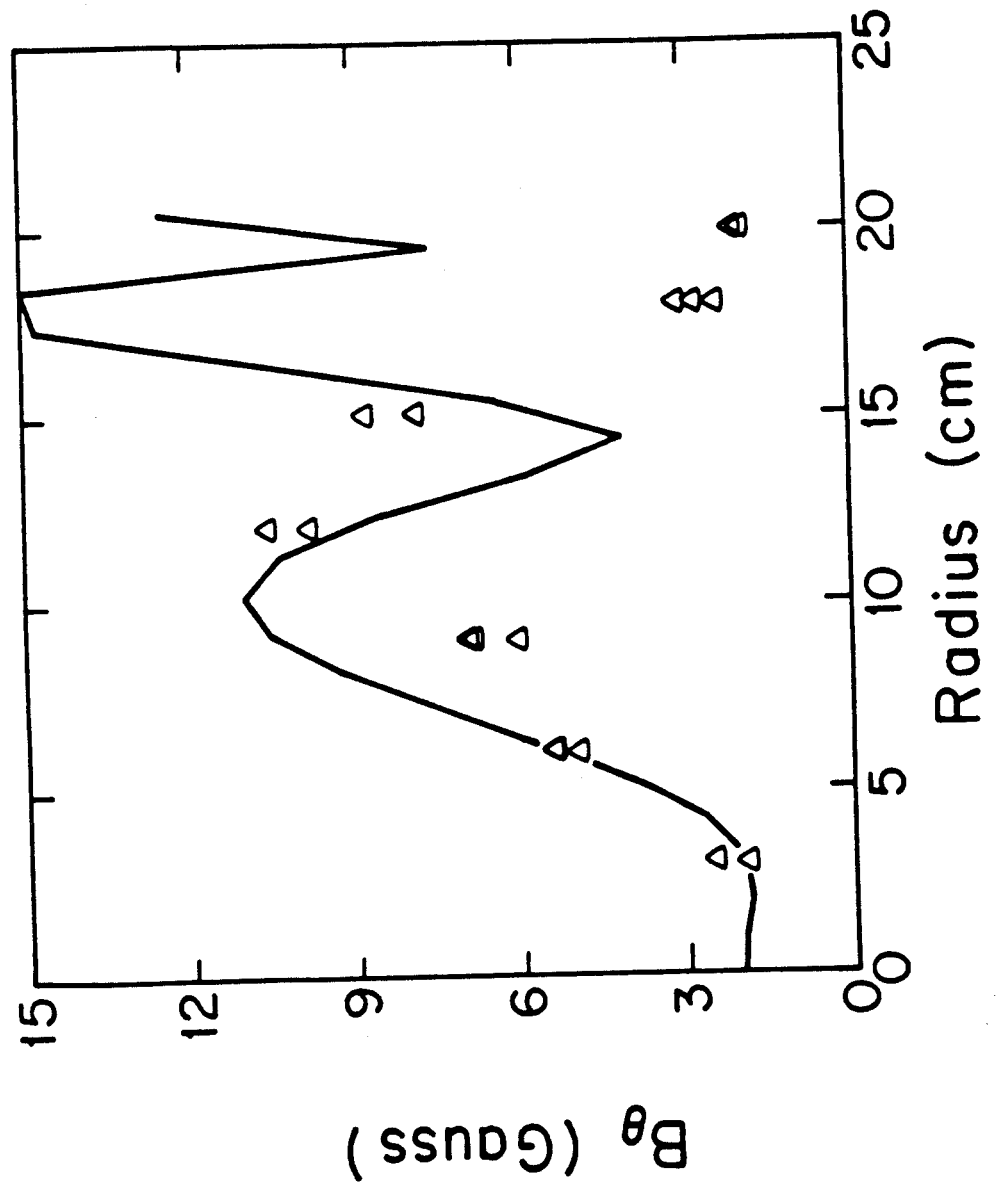

Figure 5

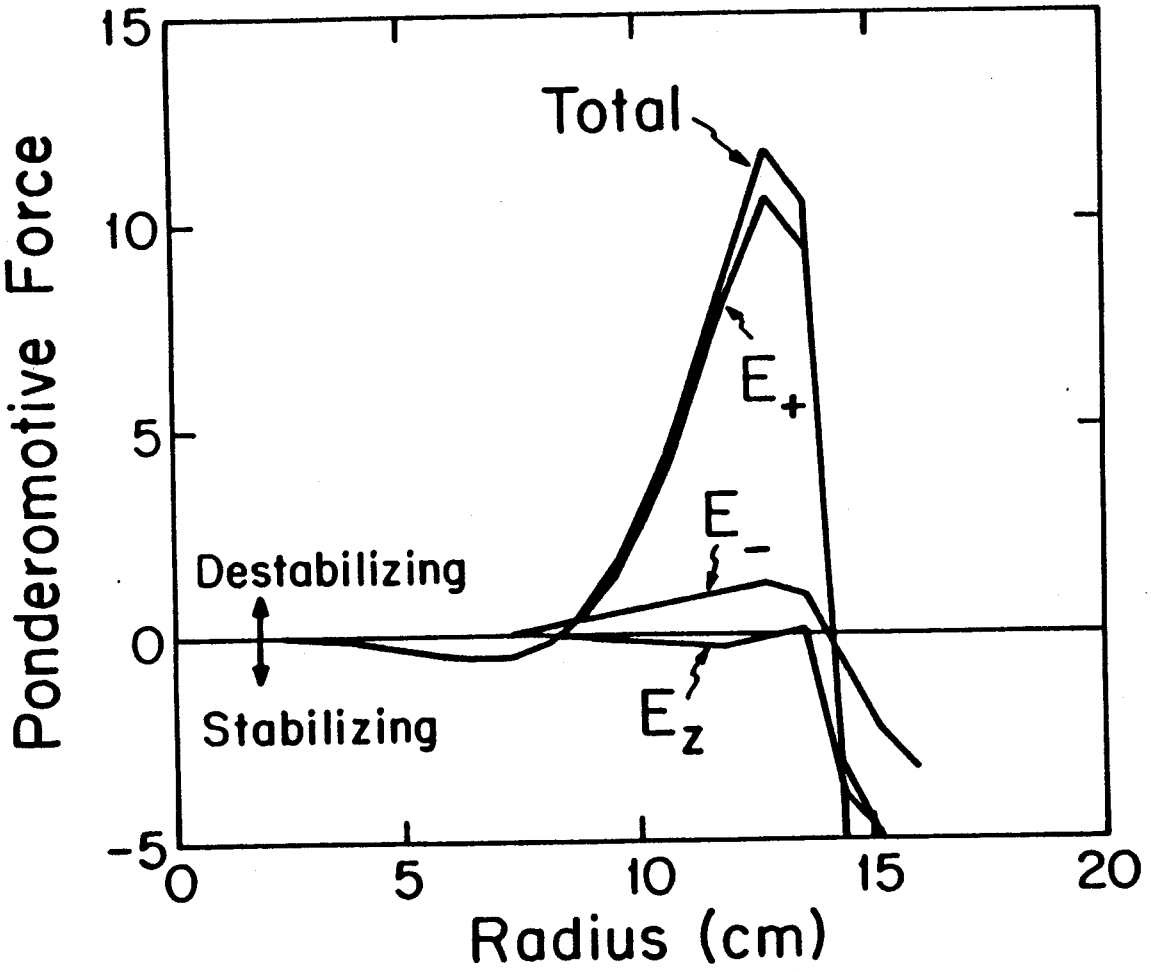
Ponderomotive Force
15
10
5
0
-5
0
5
10
15
20
Radius (cm)
Total
E+
E-
Ez
Destabilizing
Stabilizing

Figure 6

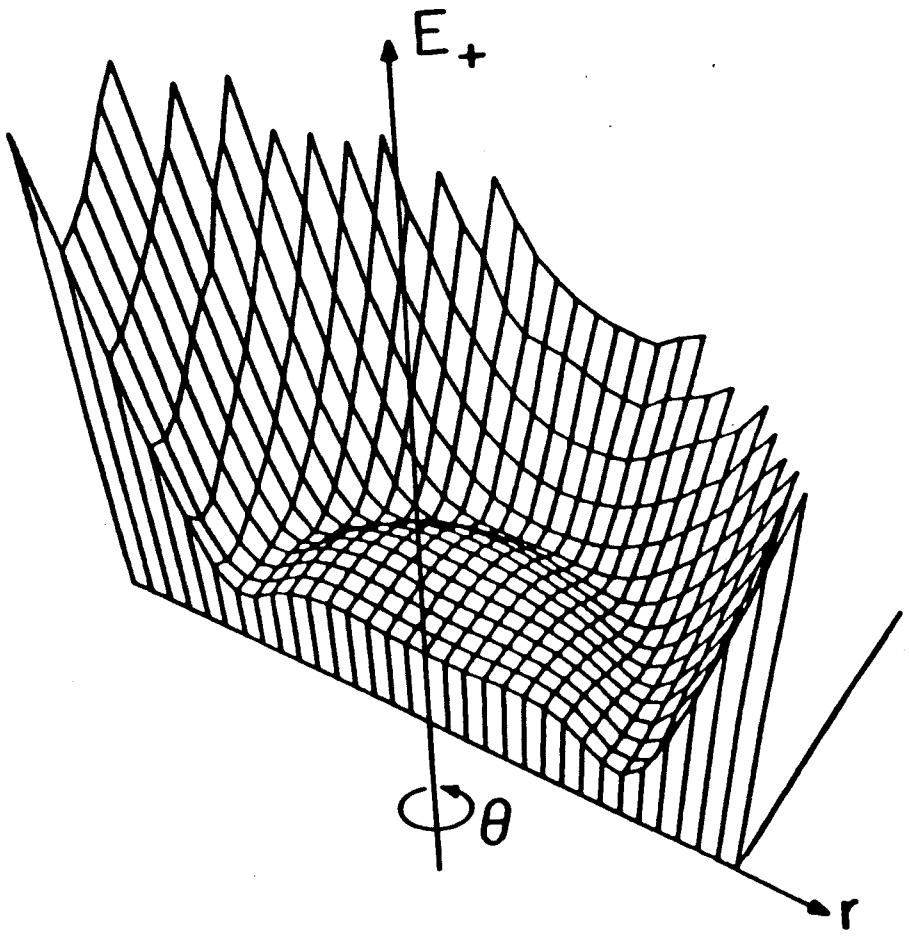

Figure 7

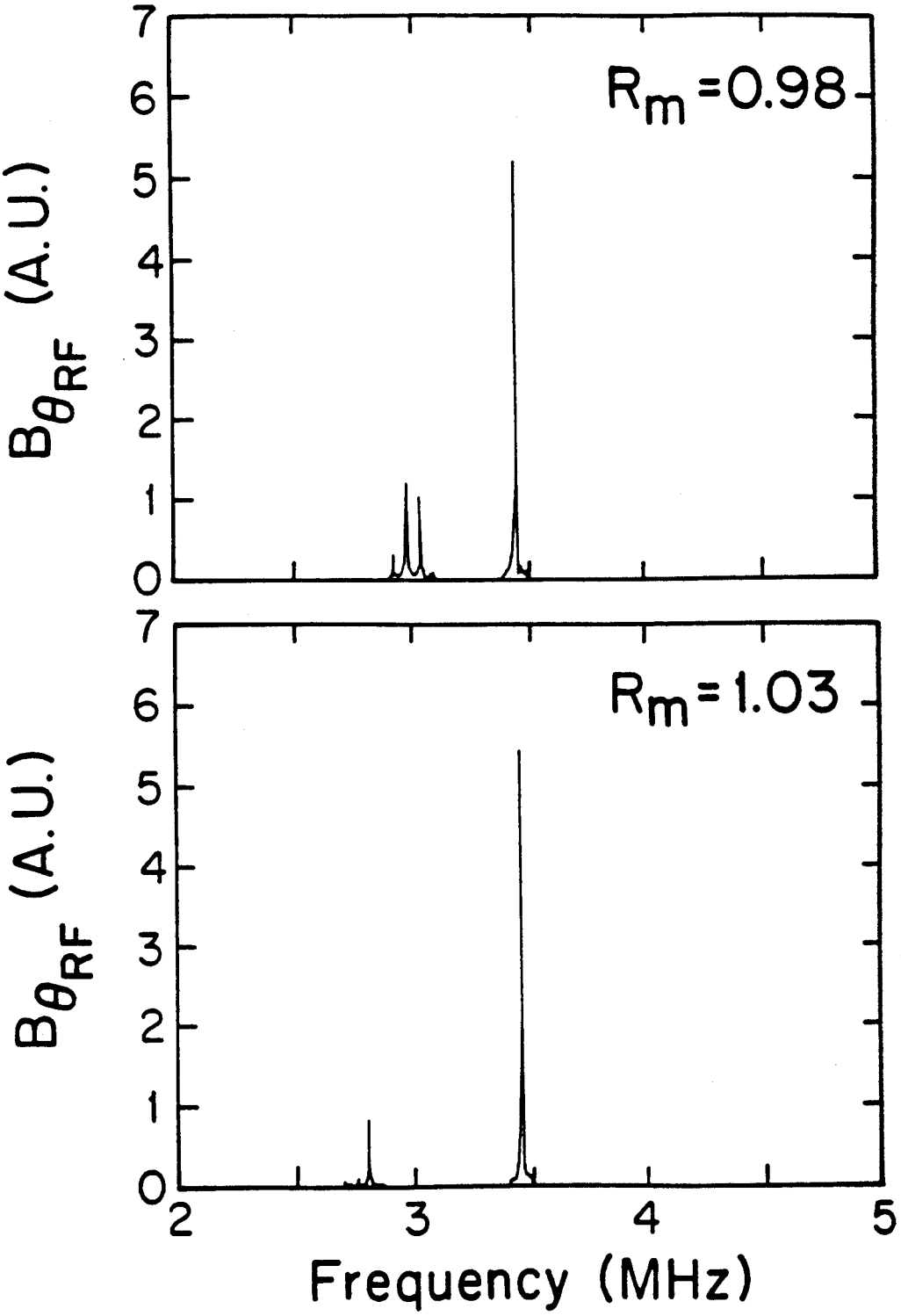
R_m = 0.98
R_m = 1.03
$B\theta_{RF}$ (A.U.)
$B\theta_{RF}$ (A.U.)
0
1
2
3
4
5
6
7
2
3
4
5
Frequency (MHz)

Figure 8

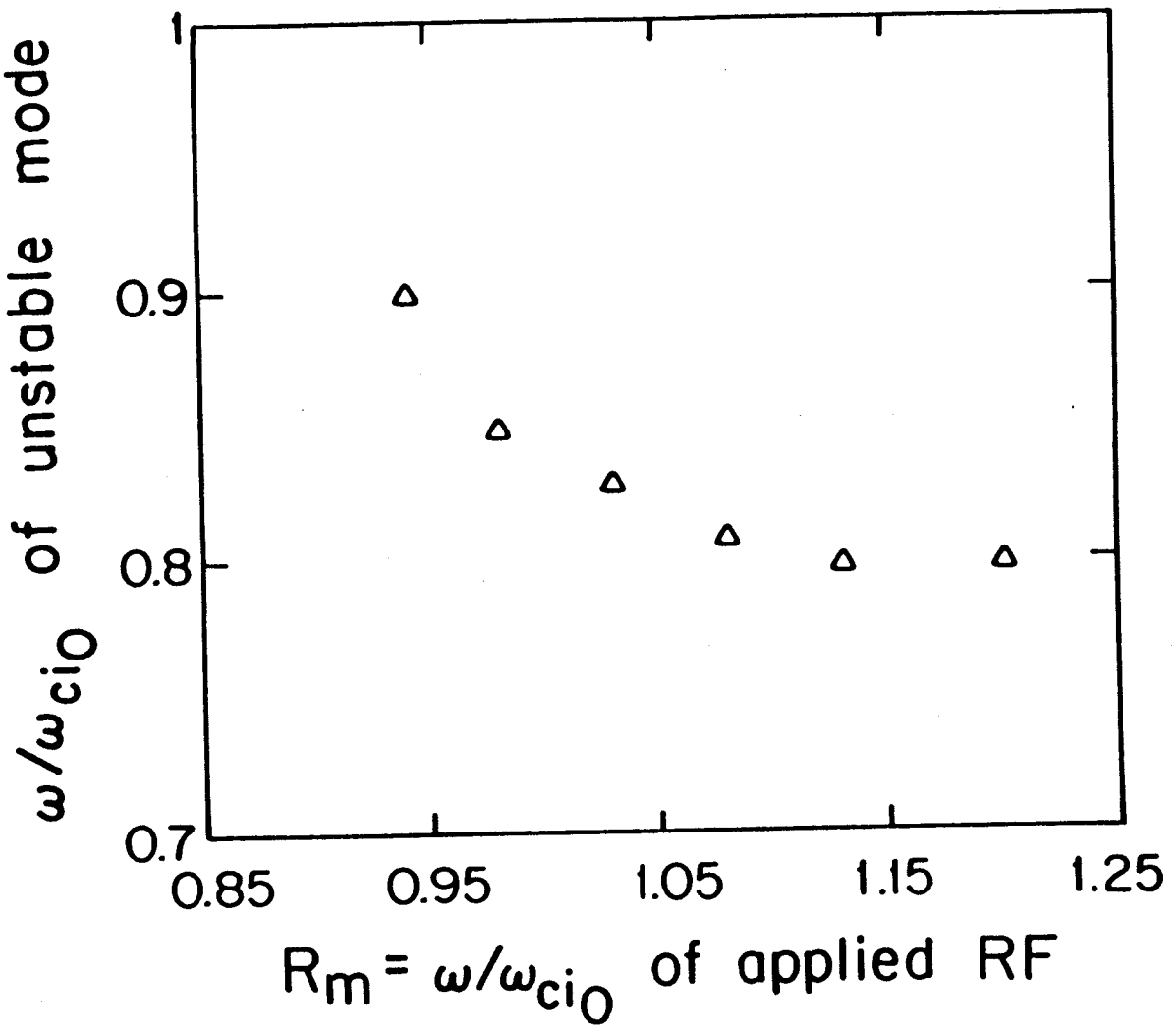
1
0.9
0.8
0.7
0.85
0.95
1.05
1.15
1.25
ω/ωci0 of unstable mode
Rm = ω/ωci0 of applied RF

Figure 9

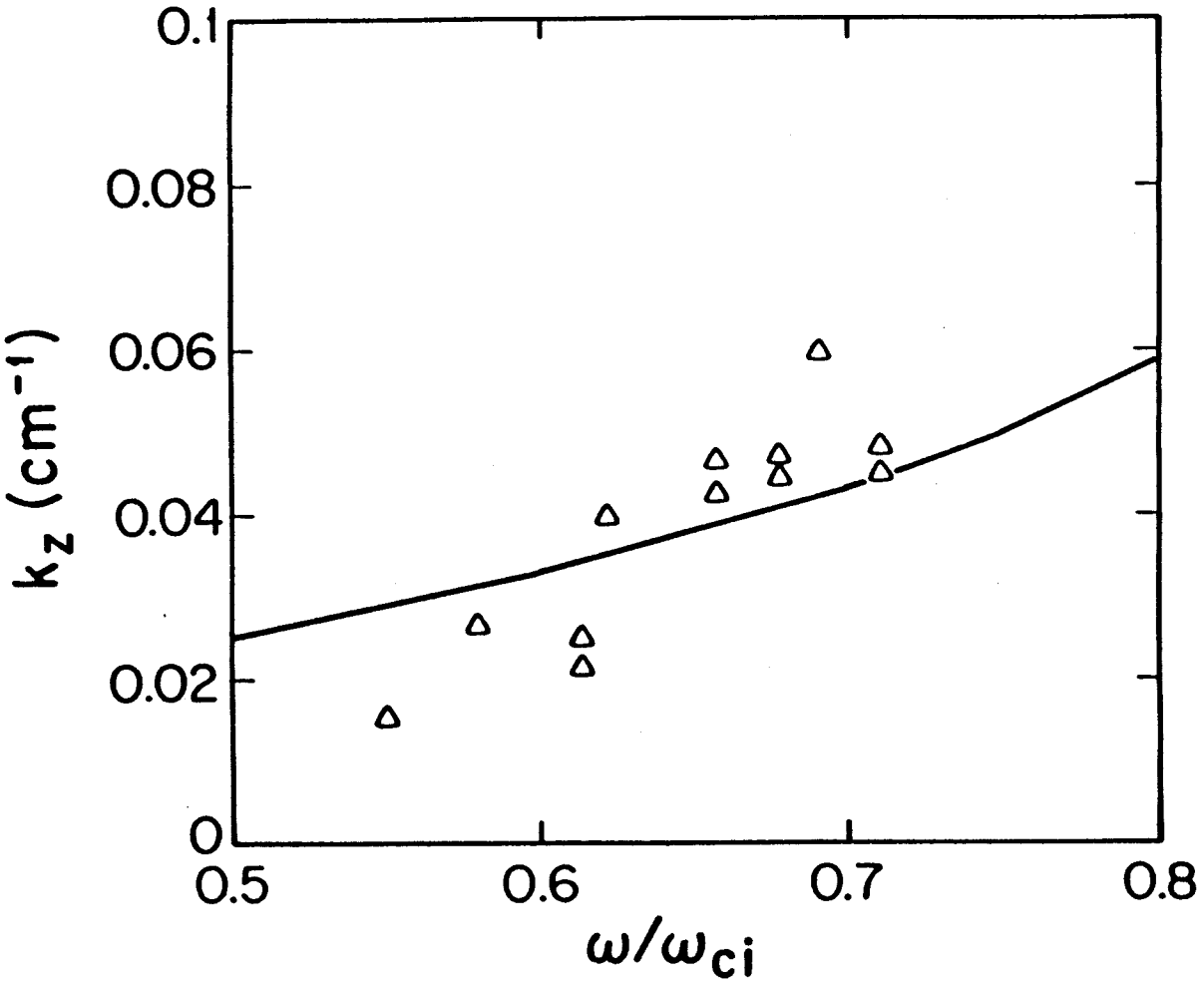

Figure 10

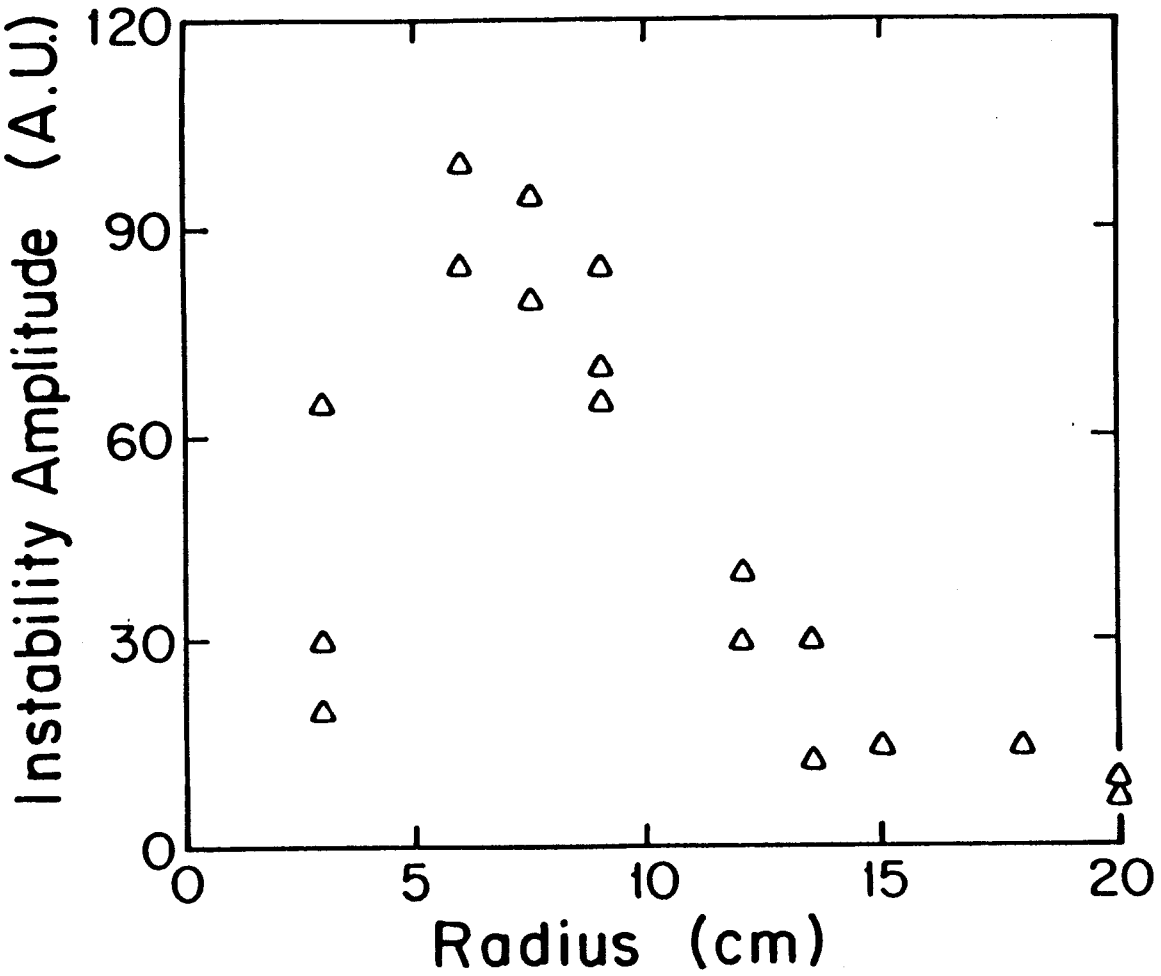

Figure 11

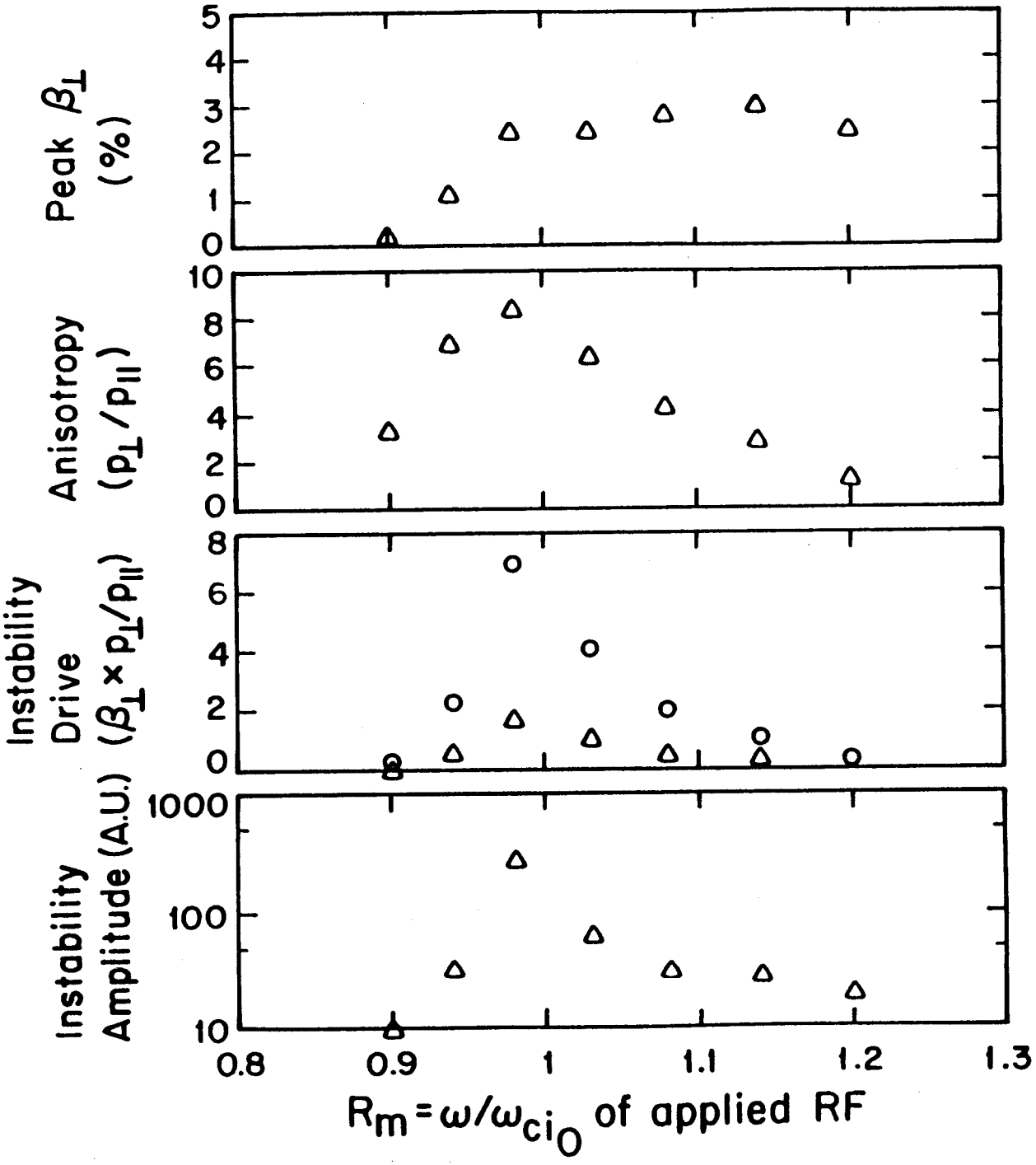
Peak $\beta_\perp$ (%)
Anisotropy ($p_\perp / p_{||}$)
Instability Drive ($\beta_\perp \times p_\perp/p_{||}$)
Instability Amplitude (A.U.)
$R_m = \omega/\omega_{ci_0}$ of applied RF

Figure 12